PCCP

Gauging van der Waals Interactions in Aqueous Solutions of 2D MOFs: When Water Likes Organic Linkers More than Open-metal Sites

Journal:	*Physical Chemistry Chemical Physics*
Manuscript ID	CP-ART-11-2020-005923.R1
Article Type:	Paper
Date Submitted by the Author:	07-Jan-2021
Complete List of Authors:	Momeni, Mohammad R.; New Jersey Institute of Technology College of Science and Liberal Arts, Zhang, Zeyu; NJIT Dell'Angelo, David; NJIT A. Shakib, Farnaz; New Jersey Institute of Technology, Chemistry and environmental Science

PCCP

ARTICLE TYPE

Cite this: DOI: 00.0000/xxxxxxxxxx

Gauging van der Waals Interactions in Aqueous Solutions of 2D MOFs: When Water Likes Organic Linkers More than Open-metal Sites†

Mohammad R. Momeni,*[a] Zeyu Zhang,[a] David Dell'Angelo,[a] and Farnaz A. Shakib*[a]

Received Date
Accepted Date

DOI: 00.0000/xxxxxxxxxx

Molecular dynamics simulations combined with periodic electronic structure calculations are performed to decipher structural, thermodynamical and dynamical properties of the interfaced vs. confined water adsorbed in hexagonal 1D channels of the 2D layered electrically conductive $Cu_3(HHTP)_2$ and $Cu_3(HTTP)_2$ metal-organic frameworks (HHTP=2,3,6,7,10,11-hexahydroxytriphenylene and HTTP = 2,3,6,7,10,11-hexathiotriphenylene). Comparing water adsorption in bulk vs. slab models of the studied 2D MOFs shows that water is preferentially adsorbed on the framework walls via forming hydrogen bonds to the organic linkers rather than by coordinating to the coordinatively unsaturated open-Cu^{2+} sites. Theory predicts that in $Cu_3(HTTP)_2$ the van der Waals interactions are stronger which helps the MOF maintain its layered morphology with allowing very little water molecules to diffuse into the interlayer space. Data presented in this work are general and helpful in implementing new strategies for preserving the integrity as well as electrical conductivity of porous materials in aqueous solutions.

1 Introduction

Conductive $\pi-$stacked 2D layered metal-organic frameworks (MOFs)[1] are a new addition to the family of nanoporous materials which offer electrical conductivity[2–5] in addition to permanent porosity and exceptionally high surface area of conventional 3D MOFs. Crystal structures of 2D MOFs are composed of tetra-coordinated semi-planar metal nodes connected through aromatic linkers creating extended $\pi-$conjugated 2D layers in *ab* plane. Stacking of layers *via* $\pi-\pi$ interactions between aromatic triphenylene rings creates parallel, noninterconnected, 1D infinite hexagonal channels along the *c* axis. This architecture provides both *in*-plane and *out*-of-plane electrical conduction as well as directional permeation of electrolyte and target molecules through the conductive material, Fig. 1. Owing to this ideal combination, unprecedented breakthroughs are made possible in producing cost-effective semiconductors;[6,7] supercapacitors;[8–11] and ion-to-electron transduced chemical sensors.[12–22] Progress towards these applications calls for a full investigation of stability of $\pi-$stacked layered MOFs subject to humidity, and possible hydrolysis of the MOF secondary building unit (SBU), and the effects of these structural transformations on the overall electrical conductivity of the material.

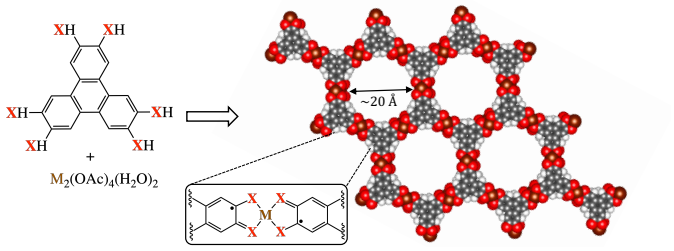

Fig. 1 Structure of 2D MOFs. Tritopic linkers and the self-assembled layered architecture along the main 1D channel with M=Cu^{2+} and X=O ($Cu_3(HHTP)_2$) and S ($Cu_3(HTTP)_2$) in this work.

When it comes to 2D MOFs, little, if not none, experimental data is available on the dynamics of confined water and its adsorption by the framework. There are many important questions to be answered; (i) What are the parameters governing the dynamics of confined water along the 1D channels versus penetration into the interlayer space; (ii) How do the van der Waals interactions reply to the presence of water within the interlayer space; (iii) Will layers be separated due to presence of water or the interlayer water will act as a glue to keep layers together?; (iv) Regardless, how will the presence of water in interlayer space affect the charge mobility between layers and the overall electrical conductivity of the 2D MOFs?; and many other such questions.

$Cu_3(HHTP)_2$ (HHTP=2,3,6,7,10,11-hexahydroxytriphenylene) is one of the first conductive 2D layered MOFs with metallic behaviour that was synthesized alongside its Co and Ni counter-

[a] Department of Chemistry and Environmental Science, New Jersey Institute of Technology, Newark 07102, NJ United States, E-mail: momeni@njit.edu, shakkib@njit.edu

† Electronic Supplementary Information (ESI) available: Details of our classical MD simulations and quantum mechanical calculations. See DOI: 10.1039/cXCP00000x/

parts in 2012.[1] In our recent study on stability of $Cu_3(HHTP)_2$ and $Co_3(HHTP)_2$ in aqueous solutions,[23] we introduced organic linker as an effective player in the dynamics of confined water in 1D channels as well as interlayer space of 2D MOFs. We expect that water is first adsorbed to the 1D channel walls *via* hydrogen bond (HB) formation with organic linkers. The flexible nature of layers and the dynamic HB network finally allows penetration of water molecules within the interlayer space. The penetrated water molecules can then form coordinative bonds with open-metal sites which leads to the increase of interlayer distance and weakening of van der Waals interactions, possibly affecting the overall integrity and electrical conductivity of the layered structure. To verify this hypothesis, here we choose to study dynamics of interface vs. confined water in the slab and bulk models of $Cu_3(HHTP)_2$ versus $Cu_3(HTTP)_2$ (HTTP= 2,3,6,7,10,11-hexathiotriphenylene), depicted in Fig. 1, as representatives of $\pi-$stacked 2D layered MOFs. We will follow the structural, thermodynamical, and dynamical footprints of water in 2D MOFs. Along the path, we will evaluate their effects on the electronic band structure of $Cu_3(HHTP)_2$ and $Cu_3(HTTP)_2$ and will differentiate the *in*-plane and *out*-of-plane charge mobility routes. These findings are transferable and applicable to other similar 2D layered nanoporous materials and are useful in designing more robust water stable materials with desired applications.

2 Methodology

A summary of our theoretical methodology is provided below with more details given in the Supporting Information (SI).

2.1 Classical molecular dynamics simulations

Classical molecular dynamics (MD) simulations for dry MOFs were initiated from the hexagonal ($\alpha = \beta = 90^\circ$, $\gamma = 120^\circ$, $a = b = 46.470$ Å, and $c = 13.555$ Å) PBE-D3 minimized tetra-layered $2\times2\times2$ supercell of the bulk $Cu_3(HHTP)_2$ and $Cu_3(HTTP)_2$ MOFs (comprised of 1008 atoms in total and 48 metal centers) using DL_POLY_2 package.[24] Force field parameters for transition metals involved in SBUs of our 2D MOFs do not exist in Generic force fields such as generalized amber force field (GAFF).[25] The first step for generating these parameters is to create a reliable training set of SBUs at *ab initio* level. Starting from the only experimentally available crystallographic data, for $Co_3(HHTP)_2$,[1] we built a $2\times2\times2$ super cell for the dry MOF by removing hydrolyzed layers, and all chemisorbed water molecules, replacing Co atoms with Cu and adjusting the interlayer distances to $\sim$4 Å. Both cell vectors and atomic positions of this supercell were then minimized with periodic boundary conditions using the Perdew–Burke–Ernzenhof (PBE)[26] density functional with damped D3 dispersion correction[27] in CP2K version 5.1.[28]. Spin polarized calculations were performed for all systems. For creating the training sets, reduced cluster models comprised of a single Cu center and two truncated linkers were cut from the optimized crystal structures (see SI Fig. S1). The central metal atoms were then displaced by 0.02 Å from -0.04 Å to +0.04 Å along the x, y and z dimensions (creating a total of 125 configurations). All electronic energies for this training set were calculated using the ωB97M-v[29] density functional and the def2-TZVP basis set as implemented in QCHEM version 5.2.[30] To fit force field parameters to this *ab initio* training set, Morse potential was used for all coordinative Cu–O and Cu–S bonds while Harmonic potential was employed for the rest. David Carrol's genetic algorithm[31] was used for fitting all bonded interactions involving the Cu^{2+} transition metal centers, including bonds, angles, and dihedrals, while all parameters related to the intramolecular interactions present in the organic linkers were taken from GAFF without further modification. The non–bonded parameters concerning transition metal sites include electrostatic as well as van der Waals interactions. To account for the former, we computed atomic charges at the ωB97X-d/def2-TZVP level[29] using the CHELPG scheme which fits all atomic charges to represent molecular electrostatic potential.[32] For the latter, Lennard-Jones parameters of Cu^{2+} were taken from the Universal Force Field (UFF).[33] More details are given in the SI section S1 as well as validation of the developed force fields are provided in SI section S2. The complete list of the bonded and non–bonded parameters for $Cu_3(HHTP)_2$ and $Cu_3(HTTP)_2$ MOFs are given in SI Tables S1-S5 and Tables S6-S10, respectively. A second 2D slab model comprised of eight layers and 2016 atoms was built for both systems to compare the properties of slab and bulk in water adsorption and dissolution. A vacuum space of 40 Å was added to the c vector of the slab models. Each system was equilibrated for 5 ns in the isothermal–isobaric NPT ensemble with a time step of 0.2 fs at 293 K temperature and 1 atm pressure, the experimental conditions at which the original 2D MOFs were synthesized,[1] allowing the simulation box to vary. The constant total energy of the systems, with less than 1 kcal/mol fluctuation confirms that 5 ns is indeed enough in order to reach an equilibrated stage. In each 1D channel of our $2\times2\times2$ supercells, there are $n = 24$ open metal sites that are exposed to confined water molecules. Therefore, to study dynamics of confined water in the bulk models, we placed $2n = 48$, $4n = 96$ and $8n = 192$ water molecules in a sphere centered at the middle of the 1D channel of the dry MOF using PACKMOL[34] code. For the slab models, a layer of water was placed in the vacuum above the slab $\sim$5 Å away from the surface. The equations of motion were propagated according to the velocity–Verlet algorithm. The temperature was kept constant using a Nosé–Hoover chain comprised of four thermostats.[35] To model water molecules, we use the flexible 4-site qTIP4P/F[36] quantum water potential which has been shown to be successful in reproducing a diverse number of static and dynamical properties of water including melting point, diffusion coefficients and IR spectrum. Dynamical properties are calculated from the average of 10 independent 50 ps NVE simulations. These trajectories were run from 10 different initial configurations obtained from 10 ps NVT trajectories that followed the NPT simulations. The final snapshots of these NVT trajectories were then used as initial configurations for 50 ps NVE simulations ensuring that different starting configurations initiate independent NVE trajectories.

2.2 Electronic structure calculations

The PBE[26] exchange-correlation functional corrected by the DFT-

D3 method of Grimme[27] as implemented in Vienna Ab Initio Simulation Package (VASP)[37–40] was used to calculate the band structure and density of states. Hubbard U corrections where U parameter is set to 10.4 eV, suggested by Gregory et al[41], are included to treat 3d states of the Cu transition metals[42–44]. Interactions between electrons and ions were described by Projector Augmented Wave (PAW) potentials[45,46] with energy cutoff set to 500 eV. Gaussian smearing was adopted in all calculations with a smearing width of 0.05 eV. The convergence criteria were 10^{-5} for self consistent field calculations and 10^{-6} for electronic property calculations. A *k*-point mesh in the Monkhorst–Pack scheme of 2×2×6 was used in the SCF part and twice denser in following calculations. Spin polarized calculations (collinear) were performed for all systems.

3 Results and Discussions

3.1 Dynamical picture of the interaction of interface vs. confined water with 2D MOFs

All hydrated systems, both bulk and slab models, were equilibrated in the isothermal-isobaric NPT ensemble for 5 ns. The equilibrated systems are provided in the SI Fig. S6 while the final equilibrated slab model of $Cu_3(HTTP)_2$, with 384 water molecules, is given in Fig. 2 as an example. Analysis of water layers in the equilibrated systems reveals five different types of water considering their interactions with the framework. Fig. 2 depicts the percentage of water molecules coordinated to one or two open-Cu^{2+} sites ($1W_{Cu}$ and $2W_{Cu}$), water molecules hydrogen bonded (HB) to one or two oxygen or sulfur atoms of the linkers ($1W_{HB}$ and $2W_{HB}$) and free water molecules (W_F) for both bulk and slab models. Calculated smaller percentage of W_Fs in slabs of $Cu_3(HHTP)_2$ compared to $Cu_3(HTTP)_2$, regardless of water concentration, clearly shows higher affinity of the former to adsorb water than the latter. Though the metal centers have the same identity in both frameworks but both $1W_{Cu}$ and $2W_{Cu}$ are negligible in $Cu_3(HTTP)_2$ slabs. Confirming our working hypothesis, HB formation with organic linkers are the first step of adsorption. As oxygen atoms of the HHTP linkers form rather stronger HBs with water molecules than sulfur of HTTP, Cu centers in $Cu_3(HHTP)_2$ are more exposed to the water molecules. Furthermore, the open-Cu^{2+} centers connected to electronegative oxygen atoms in $Cu_3(HHTP)_2$ are more positively charged compared to the open-Cu^{2+} centers connected to sulfur in $Cu_3(HTTP)_2$ (SI Tables S1 and S6). The other evidence for our hypothesis is the observed trend in $1W_{Cu}$ with respect to water concentration that closely follows the trend of $1W_{HB}$, Fig. 2. The bulk models, more or less, follow the same trends. To illustrate a more informative picture of dynamics of water, we calculated water reorientation relaxation times (τ_2 in ps) and diffusion coefficients along the interlayer space (D_{xy}) and the main 1D channel (D_z) as well as total diffusion coefficients (D_{tot}), see Table 1. We calculated D_{tot} based on the mean square displacement of the particles[47] using the following equation:

$$D = \lim_{t\to\infty} \frac{1}{6t} \langle (\mathbf{r}(t) - \mathbf{r}(0))^2 \rangle \quad (1)$$

We quantified water reorientation relaxation times in terms of the orientational time correlation functions (TCFs). Then, formulated TCFs in terms of the reorientation of the unit vector $\hat{\mathbf{u}}_{OH}$ that lies along one of the OH bonds of a water molecule:

$$C_{2,\mathrm{OH}}(t) = \langle P_2[\hat{\mathbf{u}}_{\mathrm{OH}}(0)\hat{\mathbf{u}}_{\mathrm{OH}}(t)] \rangle \quad (2)$$

where P_2 is the Legendre polynomial of order 2. The time dependence of the 2^{nd} Legendre polynomial is exponential and can be used to determine orientational relaxation time (τ_2):

$$C_{2,\mathrm{OH}}(t) \propto \exp(-\frac{t}{\tau_2}). \quad (3)$$

Table 1 Calculated water reorientation relaxation time (τ_2 in ps), diffusion coefficients along the *xy* plane (D_{xy}) and *z* direction (D_z) as well as total diffusion coefficients (D_{tot}) in $Å^2 \cdot ps^{-1}$ for bulk and slab (in parenthesis) models of 2D MOFs with different water loadings. Corresponding experimental values are provided for comparison.

	$Cu_3(HHTP)_2$			
n	τ_2	D_{tot}	D_{xy}	D_z
$1H_2O/Cu^{2+}$	18.8 (59.9)	0.063 (0.030)	0.050 (0.028)	0.089 (0.036)
$2H_2O/Cu^{2+}$	17.2 (47.1)	0.051 (0.031)	0.047 (0.029)	0.059 (0.034)
$4H_2O/Cu^{2+}$	25.4 (30.5)	0.039 (0.036)	0.033 (0.035)	0.050 (0.038)
	$Cu_3(HTTP)_2$			
n	τ_2	D_{tot}	D_{xy}	D_z
$1H_2O/Cu^{2+}$	3.1 (4.4)	0.225 (0.232)	0.149 (0.249)	0.376 (0.199)
$2H_2O/Cu^{2+}$	4.7 (4.7)	0.150 (0.165)	0.111 (0.163)	0.228 (0.167)
$4H_2O/Cu^{2+}$	5.8 (5.3)	0.106 (0.129)	0.095 (0.129)	0.126 (0.129)
Exp. bulk water	1.7–2.6[48–50]	0.229[51]		

Comparison of τ_2 values between either bulk or slab models of $Cu_3(HHTP)_2$ and $Cu_3(HTTP)_2$ again shows the free nature of water in the latter with calculated τ_2 values in the range of 3.1-5.8 ps close to that of bulk water, Table 1. In comparison, a range of τ_2 values of 17.2-59.9 ps was found for $Cu_3(HHTP)_2$. This is in line with the computed D_{tot} values which are 3-8 times higher in $Cu_3(HTTP)_2$ than $Cu_3(HHTP)_2$, Table 1. A more informative picture of water dynamics can be obtained from comparison between D_{xy} and D_z since they can shed light on water mobility into the interlayer space vs. the main 1D channel, respectively. In the case of bulk models, D_z is always higher than D_{xy} which shows water molecules cannot move as freely along the *xy* plane as the *z* direction. Focusing on bulk $Cu_3(HHTP)_2$, one can notice a decreasing trend of D_z with increasing water content. This can refer to the adsorption of water molecules by the framework where coordinated water molecules to the metal centers act as nucleation sites and draw more water within the interlayer space, overall reducing their mobility alongside the 1D channel. However, there is also a decreasing trend in D_{xy} with increasing water content. Analysis of MD trajectories, movies are provided as part of SI, shows that as the interlayer space is saturated with water, some are able to penetrate to the nearby channel but due to the high affinity of the framework for adsorbing water they still stay close to the surface. Calculated diffusion coefficients for bulk $Cu_3(HTTP)_2$ show rather similar trends to those of $Cu_3(HHTP)_2$ in spite of low affinity of the framework toward water (top panels of Fig. 2). In this case, the driving force for the dynamics of water in *xy* plane can be a network of hydrogen bonded wa-

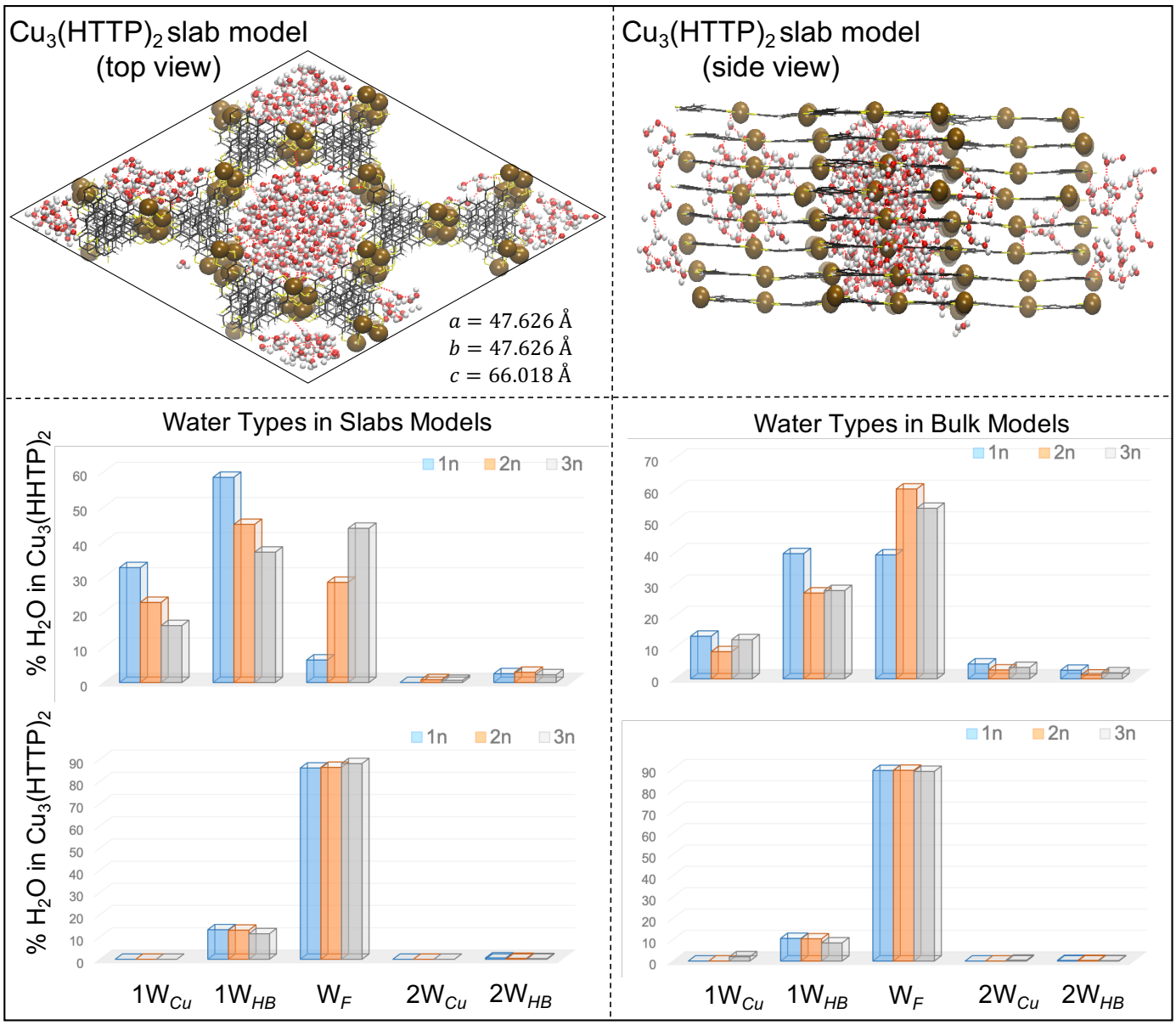

Fig. 2 Top: top and side views of representative snapshots for equilibrated slab models of $Cu_3(HTTP)_2$ with the highest water loading of 384 H_2O and with the equilibrated dimensions of the simulations box given. Calculated percentage different types of water molecules in the slab (left) and bulk (right) models of $Cu_3(HHTP)_2$ (middle) and $Cu_3(HTTP)_2$ (bottom) MOFs with different water loadings. *n* refers to the number of Cu^{2+} centers in the unit cell which is equal to 48 in the bulk and 96 in the slab models. Water molecules coordinated to one or two open-Cu^{2+} sites ($1W_{Cu}$ and $2W_{Cu}$), hydrogen bonded (HB) to one or two oxygen or sulfur atoms of the linkers ($1W_{HB}$ and $2W_{HB}$) as well as free water molecules (W_F) for both bulk and slab models are shown.

ter molecules that move freely between MOF layers and reaches the nearby channel. Analysis of MD trajectories confirms this hypothesis as the penetrated water molecules in the next channel now form a droplet away from the framework surface. Slab models do not behave as systematically as bulk models since water molecules experience two different environments in the *xy* direction, one is the interlayer space similar to the bulk model, the other is the interface of the slab with water in the z direction. One certain point that can be drawn from the data in Table 1 regarding slab models is that they generally show smaller D_z values than their counterpart bulk models. The reason is that incoming water molecules toward slab first disperse on the interface where there is plenty of open-metal sites without steric hindrance of an adjacent layer. This overall hinders the ability of the water molecules to enter into the main 1D channels. A combined picture of the dynamics of water in the slab and bulk models shows that in a realistic compact device, incoming water, and any substrate within, would face a physical hindrance to enter the channels of $Cu_3(HHTP)_2$. After entering the channel, their movement would still be slow due to penetration into the interlayer space. A device made of $Cu_3(HTTP)_2$ on the other hand would create less physical hindrances for the movement of water, and any other solvated substrates, however, there might be disadvantages of reduced contact time between framework and substrate if perform-

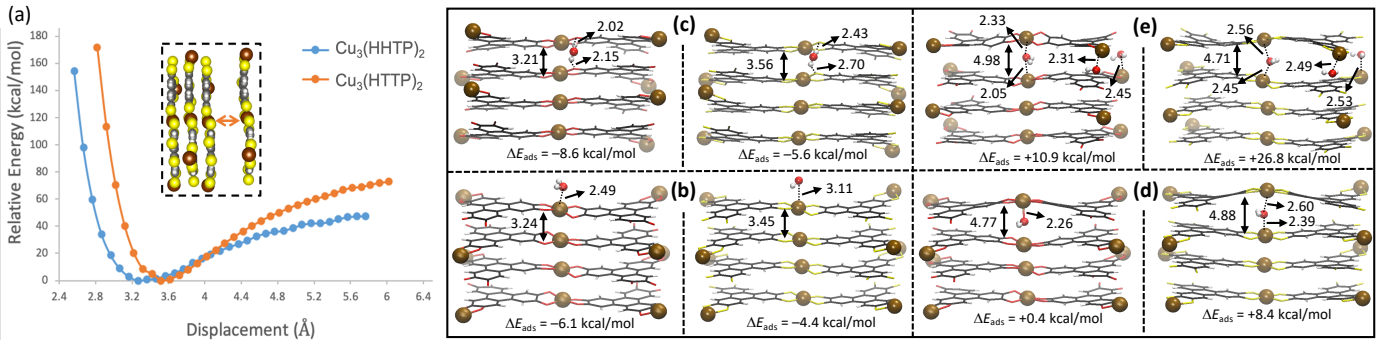

Fig. 3 (a) Calculated relative energies (kcal/mol, PBE-D3) for dry slab models of the studied 2D MOFs with minima located at 3.267 Å and 3.519 Å, representing the interlayer distances. To obtain these graphs the top outermost layers are scanned starting from their respective PBE-D3 optimized geometries. (b)-(e) Key bond and interlayer distances (Å, PBE-D3) of different modes of water interacting with the slab models of the $Cu_3(HHTP)_2$ (left) and $Cu_3(HTTP)_2$ (right) 2D MOFs.

ing a catalytic reaction is of interest. In any case, penetration of water within interlayer space is evident regardless of nature of organic linkers. This is expected to lead to an increase in the interlayer distance and possibly weakening of the $\pi-\pi$ and d-π van der Waals interactions. Now, the question is how these structural changes are going to affect the overall stability and electrical conductivity of the layered framework in aqueous solutions?

3.2 Thermodynamical footprints of water on structural deformations of 2D MOFs

Our MD simulations discussed in the previous section show that penetration of water molecules within interlayer space can occur regardless of the hydrophilicity or hydrophobicity of the framework driven by the osmosis effect of the vacant nearby channels. Will this phenomenon result in the separation of layers from each other or water molecules can act as a glue to keep layers together? We turn to quantum mechanical calculations to answer this and similar questions. First, we build a 1×1×2 slab model comprised of four layers for both $Cu_3(HHTP)_2$ and $Cu_3(HTTP)_2$ 2D MOFs suitable for such calculations. To gauge and compare the strength of $\pi-\pi$ interactions in the two systems in the absence of water, the top outermost layer was scanned from 2.567 Å – 5.567 Å in $Cu_3(HHTP)_2$ and from 2.819 Å – 6.019 Å in $Cu_3(HTTP)_2$, Fig. 3(a). The minimum of energy occurs at 3.267 Å for $Cu_3(HHTP)_2$ and 3.519 Å for $Cu_3(HTTP)_2$ representing the interlayer distance in optimized structures. The plateau represent dissociation energy of the outermost layer from the slab which is ∼20 kcal/mol higher for $Cu_3(HTTP)_2$ than $Cu_3(HHTP)_2$. This indicates stronger $\pi-\pi$ interactions in the former likely due to the larger atomic radius and polarizability of sulfur compared to oxygen. Next, we use the 1×1×2 optimized slab models to investigate how water interacts with each system (Fig. 3). Panels (b) and (c) of Fig. 3 depict two different possible configurations for adsorbing water molecules at the interface of the slab with water, either by coordination to the open-metal site (panel b) or by HB formation with organic linkers (panel c). In each panel, the left figure demonstrates the structural changes in $Cu_3(HHTP)_2$ due to water adsorption while the right one depicts the corresponding data for $Cu_3(HTTP)_2$. Consistent with our MD simulations, coordination of water to the open–Cu site in $Cu_3(HHTP)_2$ is more favorable and is exothermic (as much as 1.7 kcal/mol) than $Cu_3(HTTP)_2$. As expected, adsorption of water on top of the slab at the interface does not change the interlayer distance considerably. Panel (c) of Fig. 3 reveals that adsorption of water by HB formation does not solely occur by the linkers of the outermost layer of the slab. But, the organic linkers of the immediate layer beneath are also sharing the water molecule with the linkers of the outermost layer in both MOFs, Fig. 3. Comparison between panels c and b shows that this double HB isomer is 2.5 and 1.2 kcal/mol more stable than the coordinated isomer in $Cu_3(HHTP)_2$ and $Cu_3(HTTP)_2$, respectively. This further confirms our classical MD simulation data that HB formation to the organic linkers is the major form of water adsorption (Fig. 2). We also considered the case where the confined water is penetrated within the interlayer space and is simultaneously coordinated to the open Cu site beneath the outermost layer, panels (d) in Fig. 3. The penetrated water molecule in the interlayer space is shared between two open–Cu sites which in contrast to two previous isomers is thermodynamically endothermic. The interlayer distance is expanded around 1.4 Å in the area around the coordination site in both MOFs to accommodate the incoming water molecule. This leads to weakening of the stabilizing $\pi-\pi$ interactions. Increasing the number of water molecules to one per Cu^{2+} center in one layer, *i.e.* 3 water molecules, enhances the structural deformation in both MOFs. Now, the interlayer space between two outermost layers is increased across the unit cell, panel (e) in Fig. 2. Comparing the results from panel (d) and panel (e) it does not seem probable that water is able to completely saturate the interlayer space and separate the two outermost layers. The PBE-D3 calculated ΔE_{ads}s are 10.5 and 18.4 kcal/mol more endothermic than one water adsorption in $Cu_3(HHTP)_2$ and $Cu_3(HTTP)_2$, respectively. On the other hand, the higher ΔE_{ads} of $Cu_3(HTTP)_2$ than $Cu_3(HHTP)_2$, +26.8 vs. +10.9 kcal/mol, confirms the less affinity of the former for interacting with water molecules illustrating its higher stability in aqueous solutions.

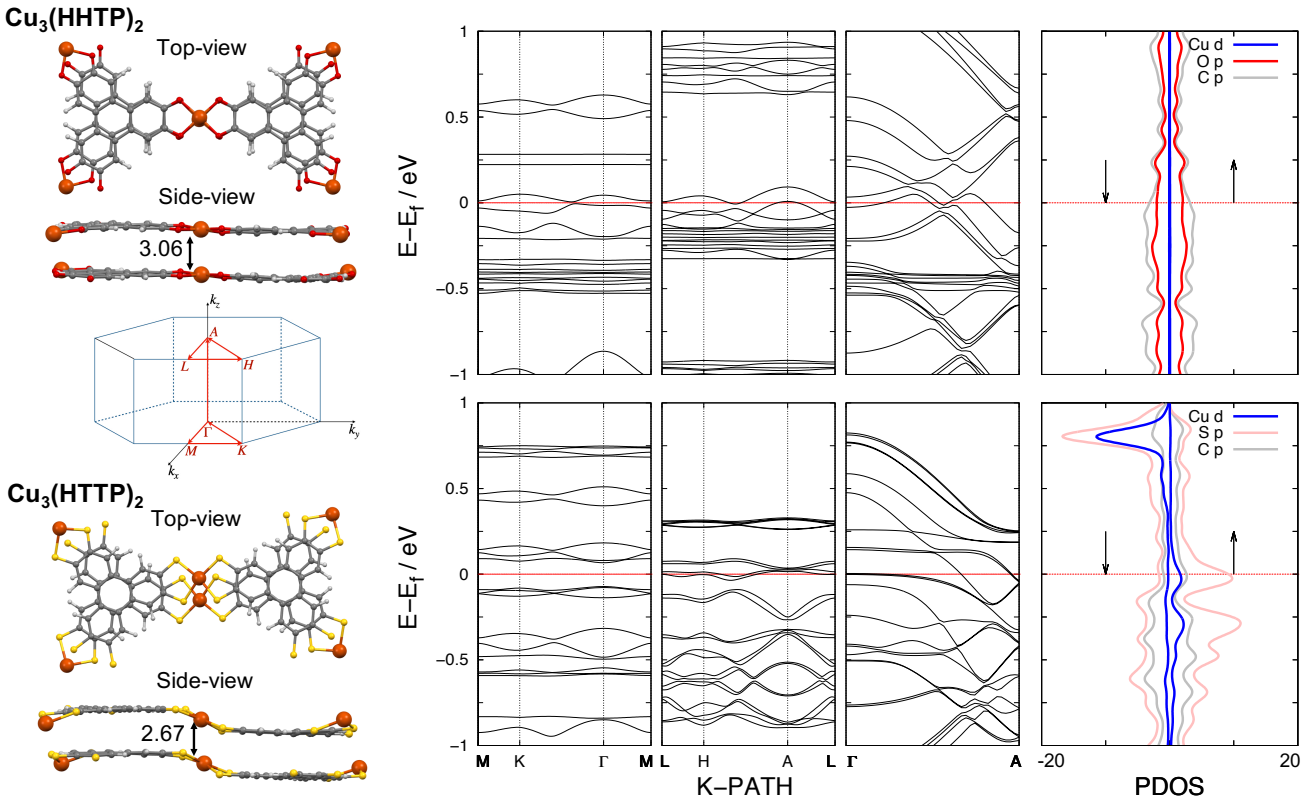

Fig. 4 Band structures and projected density of states (PBE+U, spin polarized) of the dry 1×1×1 $Cu_3(HHTP)_2$ (top) and $Cu_3(HTTP)_2$ (bottom) bluk 2D MOFs. The Fermi level is highlighted with a dashed red line and the smallest interlayer distances (in Å) are given.

3.3 Electrical conductivity subject to interaction with water

Structural stability and resistance against hydrolysis is a key factor in application of 2D MOFs for example as electrochemical sensors in aqueous solutions. Another crucial aspect in this regard is the change of electrical conductivity subject to interaction with water which calls for a full investigation at the atomistic level. Generally, the layered architecture of 2D MOFs creates two charge transport (CT) pathways, (i) extended–conjugation pathway which originates from the overlap between *d* orbitals of the metal centers and extended $\pi-\pi$ conjugation of functional groups and organic core of linkers, and (ii) through–space CT pathway due to $\pi-\pi$ interactions between organic linkers of adjacent layers.[52] This creates in–plane vs. out–of–plane electrical conductivity where the contribution of the latter to the bulk conductivity of material is yet to be fully elucidated. Hence, to provide insights on the effects of water on both the in–plane and out–of–plane electrical conductivity, we study the electronic band structure of the hydrated vs. dry 2D MOFs separated into these two categories, Fig. 4 and 5. The contribution of frontier orbitals to the electrical conductivity will be investigated through projected density of states (pDOS). It should be noted that we opted to study the band structure and pDOS on a smaller unit cell in this section, a $1\times1\times1$ periodic bulk unit cell comprised of two layers and 126 atoms, simply in order to make the calculations tractable and feasible.

From a structural point of view, the two systems under investigation differ in two main aspects (see dry $1\times\ 1\times1$ unit cells in left–hand–side of Fig. 4). (a) Along the stacking direction (side–views in Fig. 4); the almost planar layers of $Cu_3(HHTP)_2$ with a slight dihedral torsion around the central Cu atom are in contrast to the stepped geometry of layers in $Cu_3(HTTP)_2$ with a much bigger dihedral torsion. Furthermore, there is a smaller inter–layer distance in $Cu_3(HTTP)_2$ compared to $Cu_3(HHTP)_2$ (2.67 vs. 3.06 Å) which is promising for a stronger through–space $\pi-\pi$ interaction in the latter and enhancing the out–of–plane electrical conductivity. (b) Along the extended layers (top–views in Fig. 4); the slipped layers of $Cu_3(HTTP)_2$ are in contrast to the almost fully eclipsed layers in $Cu_3(HHTP)_2$. Slipping of layers in $Cu_3(HTTP)_2$, in contrast to the shorter inter–layer distance, can potentially disrupt the out–of–plane CT by weakening the through–space $\pi-\pi$ interactions. Here, we have to emphasize that these results are obtained from optimizing the atomic positions and unit cells at 0 K. As such, they are not meant to be compared to experimental results obtained at elevated temperatures but present a qualitative picture of the striking effect of organic linkers on the electrical conductivity of 2D MOFs. The narrow band–gap and hence in–plane semiconducting nature of $Cu_3(HTTP)_2$ along the MKΓ direction, as can be seen in Fig. 4, is the direct result of the stepped geometry which is expected to disrupt charge delocalization along the layers. It is interesting that even $Cu_3(HHTP)_2$ shows semimetallic signature, as opposed to metallic nature, along both intra–layer MKΓ and LHA directions, which is qualitatively equivalent to a semiconducting signature with the difference that the valence band maximum (VBM)

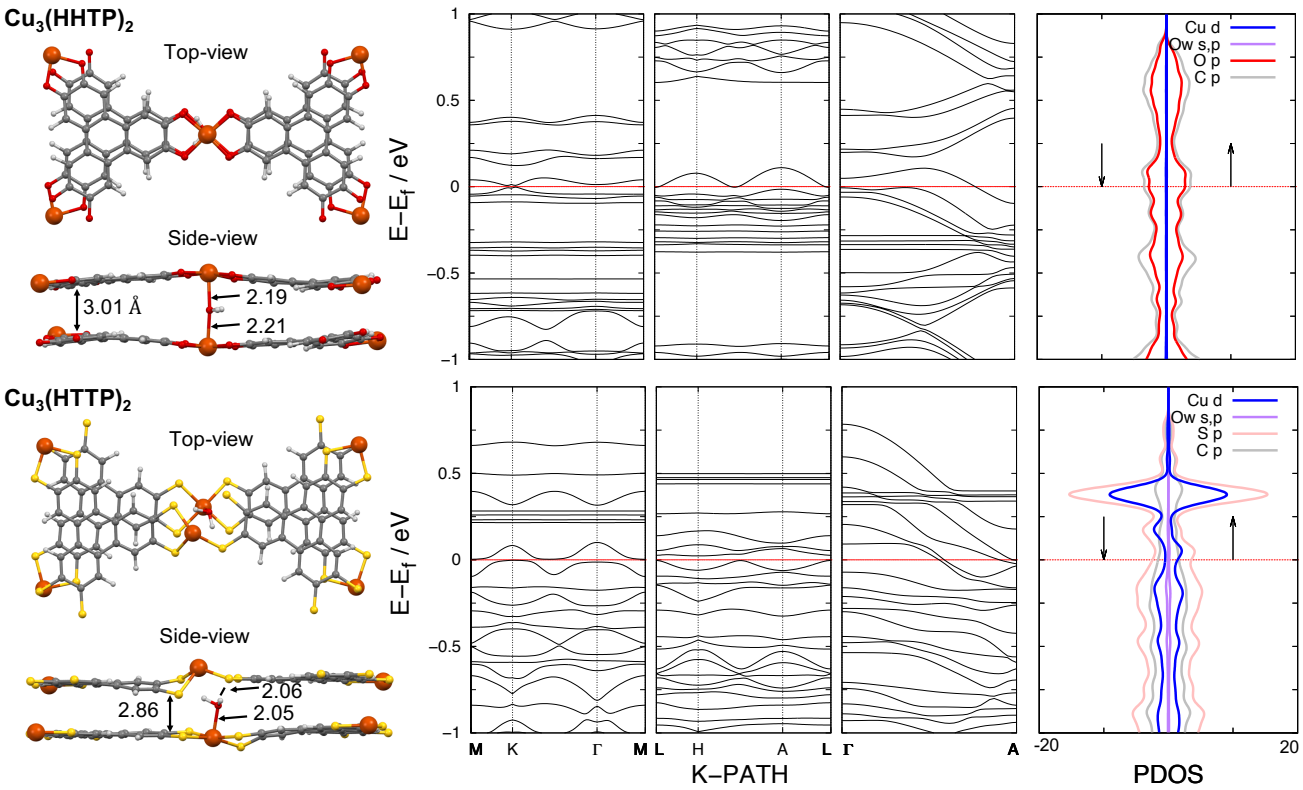

Fig. 5 Band structures and projected density of states (PBE+U, spin polarized) of the mono-hydrated 1×1×1 $Cu_3(HHTP)_2$ (top) and $Cu_3(HTTP)_2$ (bottom) bluk 2D MOFs. The Fermi level is highlighted with a dashed red line and the smallest interlayer distances (in Å) are given.

and the conduction band minimum (CBM) do not energetically overlap. The absence of well–dispersed bands in these regions is in contrast to the band transport mechanism normally expected from extended $d-\pi$ conjugated systems. Analysis of pDOS of $Cu_3(HHTP)_2$, right–hand–side of Fig. 4, shows rather similar contribution of oxygen and carbon p orbitals to the Fermi level but no contribution from d orbitals of the metal. On the other hand, $Cu_3(HTTP)_2$, shows a higher contribution of spatially extended p orbitals of sulfur to the Fermi level compared to p orbitals of carbon. The spatially extended p orbitals of sulfur atoms are also capable of forming $d-\pi$ conjugation with metal centers as evident from the contribution of the metal d orbitals to the Fermi level in this system. This is the reason behind well–dispersed bands through Fermi level in LHA direction of $Cu_3(HTTP)_2$ despite of band–gap opening in MKΓ direction. From the curvature of conduction bands and valence bands we can infer that charge mobility along the extended layers is higher for $Cu_3(HHTP)_2$ than $Cu_3(HTTP)_2$ which due to the inactive role of metal center can be attributed to hopping transport mechanism rather than band transport. Finally, the high contribution of the p orbitals of linkers to the Fermi level in both MOFs results in a well–dispersed band structure in out–of–plane direction and metallic character for both systems. This emphasizes on the importance of through space CT pathway on the electrical conductivity of the bulk material. This puts the redox–active organic linkers, as shown in Fig. 1, rather than metal center at the origin of electrical conductivity of $Cu_3(HHTP)_2$ and $Cu_3(HTTP)_2$.

The pDOS and band diagrams of hydrated 1×1×1 unit cells of $Cu_3(HHTP)_2$ and $Cu_3(HTTP)_2$ are shown in Fig. 5. They both disclose changes in charge mobility due to presence of only one water molecule between the layers which also affects their geometry appreciably. The impact on charge mobility is three fold: (a) the inter–layer dispersion is reduced, especially in the case of $Cu_3(HTTP)_2$, in agreement with previous studies[53] which shows that the increase of interlayer distance reduces the through–space $\pi-\pi$ interactions. (b) Intra–layer band gap opens up at the Fermi level along the LHA line for $Cu_3(HTTP)_2$, while in the MKΓ region the gap shrinks by going from the dry to the hydrated structure. In addition, the valleys in the conduction band suggest charge carrier traps[54] likely triggered by the the guest molecule (water). (c) The more enhanced band curvatures shows an increase of the in–plane charge mobility at the band gap. Finally, the pDOS of both systems show that water molecule does not contribute to the frontier orbitals at the Fermi level but induce structural deformations which mostly affects the in–plane electrical conductivity rather than out–of–plane.

4 Concluding Remarks

Using a combination of extensive classical molecular dynamics simulations and periodic quantum mechanical calculations the structure, dynamics and thermodynamics of the interfaced vs. confined water in bulk and slab models of 2D MOFs were carefully examined. Theory predicts that water is preferentially adsorbed on the framework walls via hydrogen bond formations with the organic linkers rather than coordination to the coordi-

natively unsaturated open-Cu^{2+} sites. Our results show that the interlayer van der Waals interactions are stronger in $Cu_3(HTTP)_2$ compared to its $Cu_3(HHTP)_2$ analogue which helps the MOF to maintain its layered morphology with allowing very little water molecules to diffuse into the interlayer space. The electrical conductivity of dry and hydrated systems were fully investigated in both in–plane (i.e. along the extended layers) and out–of–plane (i.e. along the stacking axis) directions. Analysis of band structures and pDOS revealed the important role of organic linkers in creating a through-space rather than an extended–conjugation CT pathway in both MOFs. Interaction of MOFs with water was found to affect the in–plane conductivity more drastically than the out–of–plane conductivity due to inducing geometrical changes in the extended layers.

Conflicts of interest

There are no conflicts to declare.

Acknowledgements

This work is supported by start-up fund from NJIT and used the Extreme Science and Engineering Discovery Environment (XSEDE) which is supported by NSF grant numbers CHE200007 and CHE200008. This research has been (partially) enabled by the use of computing resources provided by Kong HPC center at NJIT.

Notes and references

1 M. Hmadeh, Z. Lu, Z. Liu, F. Gańdara, H. Furukawa, S. Wan, V. Augustyn, R. Chang, L. Liao, E. Zhou, F. Perre, V. Ozolins, K. Suenaga, X. Duan, B. Dunn, Y. Yamamoto, O. Terasaki and O. Yaghi, *Chem. Mater.*, 2012, **24**, 3511–3513.

2 X. Huang, P. Sheng, Z. Tu, F. Zhang, J. Wang, H. Geng, Y. Zou, C.-A. Di, Y. Yi, Y. Sun and D. Zhu, *Nat. Commun.*, 2015, **6**, 7408.

3 L. Sun, M. Campbell and M. Dincă, *Angew. Chem., Int. Ed.*, 2016, **55**, 3566–3579.

4 A. Clough, J. Skelton, C. Downes, A. de la Rosa, J. Yoo, A. Walsh, B. Melot and S. Marinescu, *J. Am. Chem. Soc.*, 2017, **139**, 10863–10867.

5 J.-H. Dou, L. Sun, Y. Ge, W. Li, C. Hendon, J. Li, S. Gul, J. Yano, E. Stach and M. Dincă, *J. Am. Chem. Soc.*, 2017, **139**, 13608–13611.

6 D. Sheberla, L. Sun, M. Blood-Forsythe, S. Er, C. Wade, C. Brozek, A. Aspuru-Guzik and M. Dincă, *J. Am. Chem. Soc.*, 2014, **136**, 8859–8862.

7 G. Wu, J. Huang, Y. Zang, J. He and G. Xu, *J. Am. Chem. Soc.*, 2017, **139**, 1360–1363.

8 D. Sheberla, J. Bachman, J. Elias, C.-J. Sun, Y. Shao-Horn and M. Dincă, *Nat. Mater.*, 2016, **16**, 220–224.

9 W.-H. Li, K. Ding, H.-R. Tian, M.-S. Yao, B. Nath, W.-H. Deng, Y. Wang and G. Xu, *Adv. Funct. Mater.*, 2017, **27**, 1702067.

10 D. Sheberla, J. Bachman, J. Elias, C. Sun, Y. Shao-Horn and D. M., *Nat. Mater.*, 2017, **16**, 220–224.

11 D. Feng, T. Lei, M. Lukatskaya, J. Park, Z. Huang, M. Lee, L. Shaw, S. Chen, A. Yakovenko, A. Kulkarni, J. Xiao, K. Fredrickson, J. Tok, X. Zou, Y. Cui and Z. Bao, *Nat. Energy*, 2018, **3**, 30–36.

12 A. Clough, J. Yoo, M. Mecklenburg and S. Marinescu, *J. Am. Chem. Soc.*, 2015, **137**, 118–121.

13 R. Dong, M. Pfeffermann, H. Liang, Z. Zheng, X. Zhu, J. Zhang and X. Feng, *Angew. Chem., Int. Ed.*, 2015, **54**, 12058–12063.

14 E. Miner, T. Fukushima, D. Sheberla, L. Sun, Y. Surendranath and M. Dincă, *Nat. Commun.*, 2016, **7**, 10942.

15 X. Huang, H. Yao, Y. Cui, W. Hao, J. Zhu, W. Xu and D. Zhu, *ACS Appl. Mater. Interfaces*, 2017, **9**, 40752–40759.

16 X. Sun, K.-H. Wu, R. Sakamoto, T. Kusamoto, H. Maeda, X. Ni, W. Jiang, F. Liu, S. Sasaki, H. Masunaga and H. Nishihara, *Chem. Sci.*, 2017, **8**, 8078–8085.

17 L. Mendecki, M. Ko, X. Zhang, Z. Meng and K. Mirica, *J. Am. Chem. Soc.*, 2017, **139**, 17229–17232.

18 M. Yao, X. Lv, Z. Fu, W. Li, W. Deng, G. Wu and G. Xu, *Angew. Chem., Int. Ed.*, 2017, **56**, 16510–16514.

19 L. Mendecki and K. Mirica, *ACS Appl. Mater. Interfaces*, 2018, **10**, 19248–19257.

20 H. Jia, Y. Yao, J. Zhao, Y. Gao, Z. Luo and P. Du, *J. Mater. Chem. A*, 2018, **6**, 1188–1195.

21 C. Downes, A. Clough, K. Chen, J. Yoo and S. Marinescu, *ACS Appl. Mater. Interfaces*, 2018, **10**, 1719–1727.

22 Z. Meng, A. Aykanat and K. Mirica, *J. Am. Chem. Soc.*, 2019, **141**, 2046–2053.

23 Y. Shi, M. R. Momeni, Y.-J. Chen, Z. Zhang and F. A. Shakib, *Chem. Mater.*, 2020, DOI: 10.1021/acs.chemmater.0c03331.

24 T. Smith, W.; Forester, *J. Mol. Graph.*, 1996, **14**, 136–141.

25 J. Wang, R. M. Wolf, J. W. Caldwell, P. A. Kollman and D. A. Case, *J. Computat. Chem.*, 2004, **25**, 1157–1174.

26 J. P. Perdew, K. Burke and M. Ernzerhof, *Phys. Rev. Lett.*, 1996, **77**, 3865–3868.

27 S. Grimme, J. Antony, S. Ehrlich and H. Krieg, *J. Chem. Phys.*, 2010, **132**, 154104.

28 J. Hutter, M. Iannuzzi, F. Schiffmann and J. VandeVondele, *WIREs Computational Molecular Science*, 2014, **4**, 15–25.

29 N. Mardirossian and M. Head-Gordon, *J. Chem. Phys.*, 2016, **144**, 214110.

30 Y. Shao, Z. Gan, E. Epifanovsky, A. T. Gilbert, M. Wormit, J. Kussmann, A. W. Lange, A. Behn, J. Deng, X. Feng *et al.*, *Mol. Phys.*, 2015, **113**, 184–215.

31 D. Goldberg, *Genetic Algorithms in Search, Optimization and Machine Learning,*, Addison-Wesley, 1989.

32 C. M. Breneman and K. B. Wiberg, *J. Comput. Chem.*, 1990, **11**, 361–373.

33 A. K. Rappe, C. J. Casewit, K. S. Colwell, W. A. G. III and W. M. Skiff, *J. Am. Chem. Soc.*, 1992, **114**, 10024–10035.

34 L. Martínez, R. Andrade, E. G. Birgin and J. M. Martínez, *J. Comput. Chem.*, 2009, **30**, 2157–2164.

35 M. E. Tuckerman, *Statistical mechanics: Theory and molecular simulation*, (Oxford University Press, 2010.

36 S. Habershon, T. E. Markland and D. E. Manolopoulos, *J. Chem. Phys.*, 2009, **131**, 024501.

37 G. Kresse and J. Hafner, *Phys. Rev. B*, 1993, **47**, 558–561.

38 G. Kresse and J. Hafner, *Phys. Rev. B*, 1994, **49**, 14251–14269.

39 G. Kresse and J. Furthmüller, *Comput. Mater. Sci.*, 1996, **6**, 15 – 50.

40 G. Kresse and J. Furthmüller, *Phys. Rev. B*, 1996, **54**, 11169–11186.

41 G. W. Mann, K. Lee, M. Cococcioni, B. Smit and J. B. Neaton, *The Journal of Chemical Physics*, 2016, **144**, 174104.

42 V. I. Anisimov, J. Zaanen and O. K. Andersen, *Phys. Rev. B*, 1991, **44**, 943–954.

43 V. I. Anisimov, F. Aryasetiawan and A. I. Lichtenstein, *Journal of Physics: Condensed Matter*, 1997, **9**, 767–808.

44 B. Himmetoglu, A. Floris, S. de Gironcoli and M. Cococcioni, *International Journal of Quantum Chemistry*, 2014, **114**, 14–49.

45 P. E. Blöchl, *Phys. Rev. B*, 1994, **50**, 17953–17979.

46 G. Kresse and D. Joubert, *Phys. Rev. B*, 1999, **59**, 1758–1775.

47 A. Nitzan, *Chemical Dynamics in Condensed Phases: Relaxation, Transfer, and Reactions in Condensed Molecular Systems*, Oxford University Press, 2006.

48 K. Winkler, J. Lindner, H. Bürsing and P. Vöhringer, *J. Chem. Phys.*, 2000, **113**, 4674.

49 C. P. Lawrence and J. L. Skinner, *J. Chem. Phys.*, 2003, **118**, 264.

50 Y. L. A. Rezus and H. J. Bakker, *J. Chem. Phys.*, 2005, **123**, 114502.

51 K. Krynicki, C. D. Green and D. W. Sawyer, *Faraday Discuss*, 1978, **66**, 199.

52 L. S. Xie, G. Skorupskii and M. Dincă, *Chem. Rev.*, 2020, **120**, 8536–8580.

53 M. Foster, K. Sohlberg, C. Spataru and M. Allendorf, *J. Phys. Chem. C*, 2016, **120**, 15001–15008.

54 H. F. Haneef, A. M. Zeidell and O. D. Jurchescu, *J. Mater. Chem. C*, 2020, **8**, 759–787.